British Journal of Pharmacology

DOI:10.1111/bph.13282
www.brjpharmacol.org

RESEARCH PAPER

Human induced pluripotent stem cell-derived versus adult cardiomyocytes: an *in silico* electrophysiological study on effects of ionic current block

M Paci[1], J Hyttinen[1], B Rodriguez[2†] and S Severi[3†]

[1]*Department of Electronics and Communications Engineering, Tampere University of Technology, BioMediTech, Tampere, Finland,* [2]*Department of Computer Science, University of Oxford, Oxford, UK, and* [3]*Department of Electrical, Electronic and Information Engineering 'Guglielmo Marconi', University of Bologna, Cesena (FC), Italy*

Correspondence
Stefano Severi, Department of Electrical, Electronic and Information Engineering 'Guglielmo Marconi', University of Bologna, Via Venezia 52, 47521, Cesena (FC), Italy.
E-mail: stefano.severi@unibo.it

[†]Equal contribution

Received
21 April 2015
Revised
29 July 2015
Accepted
3 August 2015

BACKGROUND AND PURPOSE

Two new technologies are likely to revolutionize cardiac safety and drug development: *in vitro* experiments on human-induced pluripotent stem cell-derived cardiomyocytes (hiPSC-CMs) and *in silico* human adult ventricular cardiomyocyte (hAdultV-CM) models. Their combination was recently proposed as a potential replacement for the present hERG-based QT study for pharmacological safety assessments. Here, we systematically compared *in silico* the effects of selective ionic current block on hiPSC-CM and hAdultV-CM action potentials (APs), to identify similarities/differences and to illustrate the potential of computational models as supportive tools for evaluating new *in vitro* technologies.

EXPERIMENTAL APPROACH

In silico AP models of ventricular-like and atrial-like hiPSC-CMs and hAdultV-CM were used to simulate the main effects of four degrees of block of the main cardiac transmembrane currents.

KEY RESULTS

Qualitatively, hiPSC-CM and hAdultV-CM APs showed similar responses to current block, consistent with results from experiments. However, quantitatively, hiPSC-CMs were more sensitive to block of (i) L-type Ca^{2+} currents due to the overexpression of the Na^+/Ca^{2+} exchanger (leading to shorter APs) and (ii) the inward rectifier K^+ current due to reduced repolarization reserve (inducing diastolic potential depolarization and repolarization failure).

CONCLUSIONS AND IMPLICATIONS

In silico hiPSC-CMs and hAdultV-CMs exhibit a similar response to selective current blocks. However, overall hiPSC-CMs show greater sensitivity to block, which may facilitate *in vitro* identification of drug-induced effects. Extrapolation of drug effects from hiPSC-CM to hAdultV-CM and pro-arrhythmic risk assessment can be facilitated by *in silico* predictions using biophysically-based computational models.

Abbreviations

AL, atrial-like; APD, AP duration; APD_{ratio}, AP shape factor; EAD, early after depolarizations; hAdultV-CM, human adult ventricular cardiomyocyte; hiPSC, human-induced pluripotent stem cell; hiPSC-CM, hiPSC-derived cardiomyocyte; MDP, maximum diastolic potential; ORd, O'Hara–Rudy model of human adult ventricular cell; Paci2013, Paci model of hiPSC-CM; Rate, rate of spontaneous beating; VL, ventricular-like; V_{Max}, maximum upstroke velocity

Tables of Links

TARGETS
GPCRs[b]
β-adrenoceptors
Transporters[b]
Na^+/Ca^{2+} exchanger

LIGANDS		
Chromanol 293B	Ivabradine	Nisoldipine
Dofetilide	Mexiletine	ORM10103
E4031	Nickel	TTX
HMR-1556	Nifedipine	Zatebradine

These Tables list key protein targets and ligands in this article which are hyperlinked to corresponding entries in http://www.guidetopharmacology.org, the common portal for data from the IUPHAR/BPS Guide to PHARMACOLOGY (Pawson *et al.*, 2014) and are permanently archived in the Concise Guide to PHARMACOLOGY 2013/14 ([a,b]Alexander *et al.*, 2013a,b).

Introduction

Preclinical evaluation of the safety and efficacy of compounds before doing costly clinical trials is a major concern for pharmaceutical and cosmetic industry, regulators and society as a whole. Of major importance is the assessment of the effects of all new compounds on the heart, specifically for the identification of possible cardiotoxic side effects such as pro-arrhythmia (Heist and Ruskin, 2010; Kannankeril, 2010; Sauer and Newton-Cheh, 2012; Shah, 2013). Currently, pro-arrhythmic risk is initially assessed preclinically using ion channel assays (especially hERG assays) and evaluating the prolongation of the cardiac action potential (AP) duration, which is manifested in the ECG as the QT interval (Leishman *et al.*, 2012; Hamdam *et al.*, 2013). *In vivo* and *ex vivo* experiments using animals (rats, rabbits, dogs and non-human primates) are also used, in spite of two major limitations (Rodriguez *et al.*, 2010): (i) impaired translation from animal experiments to humans due to inter-species differences in the underlying physiology, and (ii) a lack of heterogeneity and diseased specimens in the samples considered in the experiments compared with the huge variability in the human population.

Two novel technologies have been proposed as a promising way to overcome the limitations of the existing methodologies used for preclinical safety evaluation of pharmaceutical compounds: *in vitro* experiments using human-induced pluripotent stem cell-derived cardiomyocytes (hiPSC-CMs) and *in silico* simulations using human adult ventricular cardiomyocyte (hAdultV-CM) models. The potential of both techniques, and especially their combination, has been acknowledged by the pharmaceutical industry, and also by the recent announcement by the US Food and Drug administration of a new paradigm for the evaluation of new molecular entities: 'the comprehensive *in vitro* pro-arrhythmia assay' (Sager *et al.*, 2014). The proposed scheme would include the following: (i) screening of drug action on multiple human cardiac currents (rather than just hERG) in heterologous expression systems; (ii) integration of ion channel/drug interaction data in *in silico* models of human ventricular electrophysiology to predict and evaluate changes in the human action potential; and (iii) *in vitro* evaluation of compound effects in a myocyte assay such as hiPSC-CMs and comparison to the *in silico* results. A critical point not assessed so far is how electrophysiological differences between hiPSC-CM and hAdultV-CM may result in different drug responses. Identifying these differences is critical to ensure the interpretation of combined hiPSC-CM and hAdultV-CM *in vitro*/*in silico* assays.

In this study, we have conducted the first systematic *in silico* evaluation of the effects of selective ionic current block on the APs of ventricular-like (VL) and atrial-like (AL) hiPSC-CMs and hAdultV-CMs. Our ultimate aim was to inform the potential of *in vitro* and *in silico* hiPSC-CMs technologies for preclinical drug evaluation. Our focus on selective ionic current block facilitates the systematic comparison of the different models and allows the quantification of the sensitivity of the AP to the inhibition of specific ionic currents. In our investigations we considered the most recent computational human models, which integrate existing biophysically detailed knowledge and datasets on the membrane kinetics of both hiPSC-CMs and hAdultV-CMs. We identified similarities and differences in the response of both types of cardiomyocytes to ionic current block and discuss them with regard to the underlying ionic mechanisms, in order to facilitate the interpretation of future experiments.

Methods

In silico models

Spontaneous and stimulated hiPSC-CM APs were simulated using the Paci2013 model (Paci *et al.*, 2013a), based on the comprehensive experimental dataset reported by Ma *et al.* (2011), obtained on isolated iCell hiPSC-CMs (Cellular Dynamics International, Madison, WI, USA). The Paci2013 model allows the simulation of both VL and AL hiPSC-CMs AP and includes formulations for the dynamics of ionic concentrations in the cytoplasm and sarcoplasmic reticulum, and for the kinetics of the main ionic currents and pumps, as described in the original paper. The VL and AL models were developed taking into account the differences between the main currents in ventricular and atrial phenotypes. This was performed by using scaling factors based on available data on known differences between ventricular and atrial cells. Importantly, the VL and AL models were independently validated against the morphological features of the APs for each cardiac phenotype reported previously (Ma *et al.*, 2011) (Table 1). Slight improvements in the Paci2013 model were included, as described in the Supporting Information.

Table 1

Comparison between the morphological biomarkers in spontaneous and stimulated VL hiPSC-CM and AL hiPSC-CM APs and Ca^{2+} transients

	EXP Non-stimulated (Ma *et al.*, 2011)		SIM				
			Non-stimulated		Stimulated		
	hiPSC-CM		hiPSC-CM		hiPSC-CM		hAdultV-CM
	AL	VL	AL	VL	AL	VL	
MDP (mV)	−73.5 ± 1.5	−75.6 ± 1.2	−72.2	−77.4	−71.3	−76.2	−88.0
V_{Max} ($V\,s^{-1}$)	26.2 ± 3.9	27.8 ± 4.8	24.9	26.3	33.9	47.4	259
APA (mV)	100 ± 2	104 ± 1	99.1	105	100	115	128
Peak (mV)	26.7 ± 1.4	28.3 ± 1.0	26.9	27.5	28.8	38.5	40.0
APD_{30} (ms)	123 ± 10	180 ± 11	137	212	167	258	166
APD_{50} (ms)	–	–	186	307	222	367	208
APD_{70} (ms)	–	–	229	358	267	418	240
APD_{90} (ms)	286 ± 21	415 ± 22	301	399	357	469	268
APD_{ratio}	1.1 ± 0.1 (<1.5)	2.5 ± 0.2 (>1.5)	1.09	3.16	1.09	3.41	1.60
Rate (beats min^{-1})	50.0 ± 10.0	35.3 ± 2.2	55.2	37.3	–	–	–
Diastolic Ca^{2+} (nM)	–	–	38	16	40	11	86
Systolic Ca^{2+} (nM)	–	–	296	281	241	150	368
Amplitude (nM)	–	–	258	265	201	140	282

EXP, experimental; SIM, simulated; APA, AP amplitude; Peak, peak voltage; Rate, rate of the spontaneous electrical activity; VL, ventricular-like; AL, atrial-like; hiPSC-CM, human-induced pluripotent stem cell-derived cardiomyocyte; APs, action potentials; APD, action potential duration.

In silico simulations were also conducted using the hAdultV-CM O'Hara–Rudy (ORd) endocardial model (O'Hara *et al.*, 2011). The ORd model includes a similar level of biophysical detail as the Paci2013 model.

AP assessment

Action potentials were evaluated at steady-state, after 900 s of simulation. The following morphological AP biomarkers were quantified: AP amplitude, AP duration at several repolarization percentages (APD_{30}, APD_{50}, APD_{70}, and APD_{90}), maximum diastolic potential (MDP), maximum upstroke velocity (V_{Max}), peak voltage and spontaneous beating rate. The shape factor

$$APD_{ratio} = \frac{APD_{30} - APD_{40}}{APD_{70} - APD_{80}}$$

discriminates between VL and AL hiPSC-CM APs: as in Ma *et al.*, (2011), an AP is considered VL if $APD_{ratio} > 1.5$ and AL if $APD_{ratio} < 1.5$. Details about the stimulation protocols are reported in the Supporting Information.

For each biomarker, the % variation induced by blocking each ionic current was computed (Tables 2, S1, S2 and S3). Then, considering only one model at a time, we normalized the variations in each specific biomarker with respect to the largest one (the most positive one for positive variations or the most negative one for negative variations) within all ionic current blocks (Figures 5, 6 and S2). To compare VL hiPSC-CM and hAdultV-CM, we repeated the previous procedure considering the % variations for both models (Figure 7).

In silico simulation of ionic current block

Specific block of I_{Na}, I_{CaL}, I_f, I_{K1}, I_{Kr}, I_{Ks}, I_{to} and I_{NaCa} was assessed on stimulated APs. As in previous studies (Brennan *et al.*, 2009; Davies *et al.*, 2012; Zemzemi *et al.*, 2013), drug block was simulated using a simple pore block model affecting the relevant maximum conductances based on a dose–response curve for each of the ionic currents, I, as follows:

$$\frac{I[D]}{I} = \frac{1}{1 + \frac{[D]}{IC_{50}}}$$

where $[D]$ represents the current blocker concentration, IC_{50} is the drug concentration leading to 50% of block and the Hill coefficient is assumed to be one. This particular model aids in the interpretation of our results for selective drugs. For each current, four different degrees of block were tested, 0.1 × IC_{50}, IC_{50}, 2 × IC_{50} and full block, corresponding to current block levels of 9, 50, 67 and 100%. From steady-state conditions, the maximum conductance of each current was reduced according to the specific concentration of the blocker. Simulations were then run for an additional 300 s, after which the APs were assessed and the aforementioned biomarkers were quantified. In the case of I_{Kr} block, APs were assessed after 7 s from block, because for longer simulations, repolarization failure was observed in some cases (at 2 × IC_{50} in AL hiPSC-CM and at full block in VL and AL hiPSC-CM and hAdultV-CM).

Numerical simulations

The Paci2013 model was implemented in MATLAB Simulink (The MathWorks, Inc., Natick, MA, USA), whereas the ORd model was implemented in MATLAB. Both models were solved using ode15s.

Table 2

Comparison between the % changes caused by each ionic current block in the AP biomarkers quantified by the VL hiPSC-CM and the hAdultV-CM AP models

		Variation (%)								
		MDP	V_{Max}	APA	Peak	APD_{30}	APD_{50}	APD_{70}	APD_{90}	APD_{ratio}
I_{Na}	VL hiPSC-CM	1	−53	−7	−23	14	3	0	1	−20
	hAdultV-CM	0	−69	−3	−8	3	2	2	1	0
I_{CaL}	VL hiPSC-CM	0	5	0	2	−82	−73	−68	−66	−35
	hAdultV-CM	0	3	−2	−5	−24	−21	−17	−16	−5
I_{Kr}Ad	VL hiPSC-CM	0	−35	−6	−17	63	64	59	56	38
	hAdultV-CM	0	0	0	1	45	56	67	66	2
I_{Kr}SS	VL hiPSC-CM[a]	−2	−48	−2	−2	96	86	79	69	58
	hAdultV-CM[a]	0	1	0	1	32	39	45	44	16
I_{Ks}	VL hiPSC-CM	0	−1	0	−1	3	2	2	2	4
	hAdultV-CM	0	0	0	0	5	4	4	4	−5
I_{K1}	VL hiPSC-CM	−16	−65	−14	−12	30	22	34	50	−73
	hAdultV-CM	0	2	1	1	0	0	1	7	−28
I_f	VL hiPSC-CM	1	21	4	9	1	3	3	4	6
	hAdultV-CM	–	–	–	–	–	–	–	–	–
I_{NaCa}	VL hiPSC-CM	−1	−1	2	6	11	1	−3	−8	24
	hAdultV-CM	0	1	0	1	−10	−11	−10	−9	−18
I_{to}	VL hiPSC-CM	0	−2	1	2	2	2	2	2	7
	hAdultV-CM	0	0	2	5	−2	−1	0	0	17

The 2 × IC_{50} concentration was considered, except where specified. The % variations with respect to the control values of each biomarker are reported. Two rows are reported for I_{Kr}: Ad contains biomarkers 7 s after administration of the blocker, while SS refers to the steady-state.
[a]IC_{50} concentration is considered.
EXP, experimental; SIM, simulated; APA, AP amplitude; Peak, peak voltage; Rate, rate of the spontaneous electrical activity; VL, ventricular-like; AL, atrial-like; hiPSC-CM, human-induced pluripotent stem cell-derived cardiomyocyte; APs, action potentials; APD, action potential duration.

Results

Spontaneous and stimulated control hiPSC-CM APs

The time course of the simulated VL and AL hiPSC-CM APs and the underlying ionic currents is illustrated in Figures 1 and 2 at steady-state, for spontaneous and stimulated APs, respectively. Table 1 presents the quantitative comparison between the biomarkers obtained from experimental spontaneous APs as reported in Ma *et al.*, (2011) and those quantified from the *in silico* simulations. Both models yielded values for the biomarkers consistent with experimentally-reported ranges. Moreover, the main differences between VL and AL APs were successfully simulated, including an APD_{ratio} of 3.16 and 1.09 and the higher spontaneous beating rate of AL compared with VL hiPSC-CMs, as reported by Moretti *et al.*, (2010), Ma *et al.*, (2011) and Lahti *et al.*, (2012).

The last three columns of Table 1 provide a comparison between the biomarkers from stimulated hiPSC-CM and hAdultV-CM APs simulations. Simulated hiPSC-CM exhibited depolarized MDP values (by ~12 mV), decreased AP amplitude and longer APD than hAdultV-CM, with values consistent with the experimental data reported by Li *et al.* (1998) and Moretti *et al.* (2010).

Effects of ionic current block on hiPSC-CM and hAdultV-CM AP

Figures 3 and 4 show the stimulated APs for VL hiPSC-CM, AL hiPSC-CM and hAdultV-CM in control conditions and for the four degrees of block of I_{Na}, I_{CaL}, I_f, I_{K1} and I_{Kr}, I_{Ks}, I_{to} I_{NaCa}. Biomarker values are summarized in Figures 5 and 6 for VL and AL hiPSC-CM and in Figure S2 for hAdultV-CM. A specific comparison of the variations induced by 2 × IC_{50} block in VL hiPSC-CM and hAdultV-CM APs is presented in Figure 7. Numerical values are presented in Table 2, and in the Supporting Information, Tables S1–S3. Stimulated APs are also compared with spontaneous ones in Tables S4 and S5, showing that the biomarker changes are quite consistent.

I_{Na} block. Specific I_{Na} block is usually obtained by means of tetrodotoxin (Ma *et al.*, 2011) or mexiletine (Ma *et al.*, 2013). As expected, in all cell types I_{Na} block affected primarily the AP upstroke, and, therefore, V_{Max} and AP amplitude (Figures 3A, S1 and Tables 2, S1–S5). V_{Max} was strongly reduced by I_{Na} block in both hiPSC-CMs (up to −78%). The peak voltage was affected as well, and the VL hiPSC-CM was found to be more sensitive than the AL hiPSC-CM.

Similar effects of I_{Na} block were observed in the hAdultV-CM upstroke (Figure 3A and Tables 2 and S3), including a dramatic decrease in V_{Max} with the highest levels of block (up to −69%). The peak voltage was slightly less sensitive to I_{Na} block in simulated hAdultV-CM than in VL hiPSC-CM. For full block, the stimulus current had to be increased from 80 to 140 $pA \cdot pF^{-1}$ to trigger an AP due to a significant reduction in excitability.

I_{CaL} block. I_{CaL} has a critical role in sustaining the AP plateau and therefore the APD. In *in vitro* experiments, it is selectively blocked by using nifedipine (Ma *et al.*, 2011) or nisoldipine.

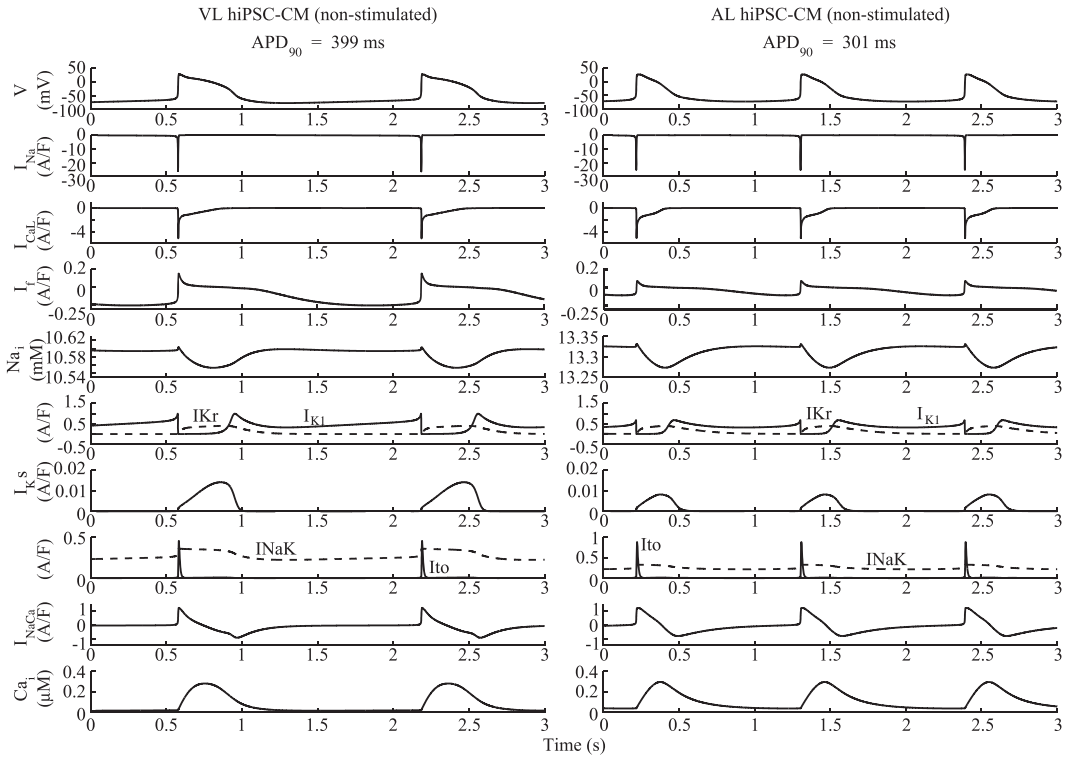

Figure 1

Simulated spontaneous VL (left) and AL (right) hiPSC-CM action potentials, ionic currents and concentrations. No external stimulus was used (I_{stim} = 0).

In our simulations, the I_{CaL} block-induced APD shortening was evident in all models, although it was larger in hiPSC-CMs than in hAdultV-CM (over 68% vs. less than 30% for full block) (Figure 3B and Tables 2, S1–S5). Of note, due to a marked APD shortening, the spontaneous beating prevailed on pacing at 80 beats·min^{-1} for the AL hiPSC-CMs, therefore the pacing rate was increased to 100 beats·min^{-1}.

We hypothesized that such a different AP shortening in VL hiPSC-CM and hAdultV-CM is induced by differences in the I_{NaCa} between the two models. To test this hypothesis, we replaced the I_{NaCa} formulation in the hAdultV-CM model by the one in the VL hiPSC-CM. The simulations then showed that APD after I_{CaL} block was close to that obtained in VL hiPSC-CM (Figure S4, green vs. blue curves). Comparing the time course of I_{NaCa} during the AP in the original hiPSC-CM model and in the hAdultV-CM model with the hiPSC-CM I_{NaCa} formulation under I_{CaL} full block conditions (not shown) shows that the current profiles are similar but the amplitude of the current (both in outward and inward modes) is 3.2 times larger in hiPSC-CM than in hAdultV-CM. We then increased the maximal I_{NaCa} current by 3.2 times and tested the I_{CaL} full block again, which showed that the I_{NaCa} increase was almost fully responsible for the APD shortening obtained within the hAdultV-CM model with the hiPSC-CM I_{NaCa} formulation (see in Figure S4 the red curve almost superimposed to the green one). Finally, we also tested the effect of the persistent component of the sodium current I_{NaL} (not present in the hiPSC-CM models) in preserving the APD in hAdultV-CM in conditions of I_{CaL} block. By fully blocking the I_{NaL} and I_{CaL} at the same time in the hAdultV-CM model with the hiPSC-CM I_{NaCa} formulation, an even larger APD_{90} reduction was achieved that almost equalled the shortening shown in hiPSC-CM after I_{CaL} block (see in Figure S4 the magenta curve almost superimposed to the blue one). The analysis therefore suggests that the differences in the response of hAdultV-CM and hiPSC-CM to I_{CaL} block are due to differences in I_{NaCa} and I_{NaL} currents.

I_{Kr} and I_{Ks} block. As shown in Figure 4A and Tables 2, S1–S5, I_{Kr} block induces a strong APD prolongation for all cell types, at all repolarization phases. A similar APD prolongation was obtained using E4031 (Ma *et al.*, 2011) or dofetilide. At the IC_{50} concentration, the APD_{90} increased by about +40% for all the three models. Full I_{Kr} block induced an even more dramatic prolongation of APD_{90}, +90% and more for both hiPSC-CMs, and for hAdultV-CM, early after depolarizations (EADs) were triggered. Note the strong decrease in V_{Max} caused by I_{Kr} block in hiPSC-CMs, which was due to the fact that APD prolongation reduces the diastolic interval and therefore limits the I_{Na} recovery from inactivation and its availability to trigger the next AP. In VL hiPSC-CM, for 2 × IC_{50} I_{Kr} block, only 6% of I_{Na} current was available (computed as product of the inactivation gating variables *h* and *j*) at the end of the diastolic phase. The V_{Max} drop observed in VL hiPSC-CM was not seen for hAdultV-CM, in which I_{Na} had sufficient time to recover from inactivation even after I_{Kr} block-induced AP prolongation because, in spite of the similar % prolongation, the absolute APD_{90}

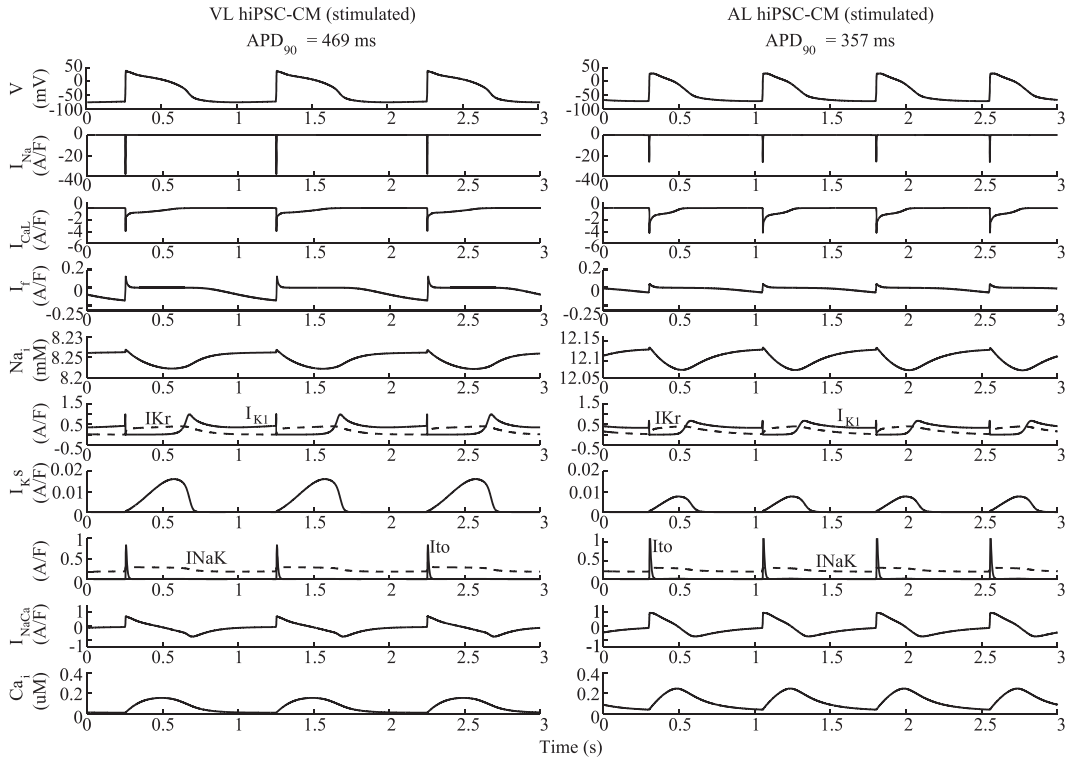

Figure 2

Simulated VL (left) and AL (right) hiPSC-CM action potentials, ionic currents and concentrations under stimulation at 60 (VL) and 80 beats min^{-1} (AL).

value was significantly shorter in hAdultV-CM than in VL hiPSC-CM (446 ms vs. 732 ms at 2 × IC_{50}).

In Ma *et al*, (2011), 3R4S-Chromanol 293B was used for I_{Ks} block but its influence on I_{to} was also reported (Thomas *et al*., 2003). In Thomas *et al*., (2003) and So *et al*. (2008), HMR-1556 resulted a more selective blocker of I_{Ks}, with influence on other currents only at high concentrations. Simulations demonstrated only a minor effect of I_{Ks} block on the AP shape for both hiPSC-CMs and hAdultV-CM (Figure 4B and Tables 2, S1–S5), with APD_{90} shortening <3% for full block. This is also due to the fact that in our *in silico* analysis, the effect of stimulation of β-adrenoceptors was not considered.

I_{K1} block. Simulations show the importance of I_{K1} in maintaining the MDP in all cell types but with significant quantitative differences (Figure 3D and Tables 2, S1, S2, S4 and S5). I_{K1} block, which can be performed *in vitro* by means of $BaCl_2$ (Sartiani *et al*., 2007), resulted in an elevated MDP (over 9%) in both hiPSC-CMs, and as a consequence, reduced I_{Na} availability and a severe reduction in V_{Max} by over 50% for IC_{50} block. The influence of I_{K1} on APD was also strong for both hiPSC-CMs, especially for APD_{90}, which was prolonged at the IC_{50} by 28% in VL hiPSC-CM and by 58% in AL hiPSC-CM. Figure 3D shows the repolarization failure that immediately followed the full I_{K1} block in both the hiPSC-CM models (and 2 × IC_{50} block only for AL hiPSC-CM).

The hAdultV-CM simulations show a very stable MDP for the three lowest degrees of I_{K1} block (Figure 3D and Tables 2, S3). In contrast, a complete block induced a marked slowdown of the late repolarization with consequent APD_{90} prolongation, and this was followed by a slight hyperpolarization (+5%) of MDP.

To understand the different behaviours in VL hiPSC-CM and hAdultV-CM, we performed additional *in silico* analyses to evaluate the role of I_{Kr} in compensating for the lack of a repolarizing effect of I_{K1} in hAdultV-CM versus VL hiPSC-CM. As reported in Figure S5A and S5B, the peak I_{Kr} under AP was half in VL hiPSC-CM with respect to hAdultV-CM (0.4 vs. 0.86 $pA{\cdot}pF^{-1}$) and it was not enough to repolarize the AP in the case of I_{K1} block. To confirm this result, we simulated, in conditions of full block of I_{K1}, the effect of doubling I_{Kr} in hiPSC-CM (Figure S5C) and halving the I_{Kr} in hAdultV-CM (Figure S5D). Figure S5C shows in VL hiPSC-CM how a doubled I_{Kr} partly compensates for the absence of I_{K1}, and restores repolarization. In contrast, Figure S5D illustrates that in hAdultV-CM, reducing I_{Kr} enhances the effects of I_{K1} block, especially during the late repolarization.

I_f block. I_f can be blocked by means of zatebradine (Sartiani *et al*., 2007) or ivabradine. Figure 3C and S3 show that I_f block has only minor effects on the AP shape in both hiPSC-CMs, whereas it cannot be simulated in hAdultV-CM because it lacks I_f. However, in VL hiPSC-CM, it has some enhancing effects on MDP, V_{Max} and peak voltage (Figure 5 and Tables 2, S1, S2, S4 and S5). As shown in Figure 2, I_f is stronger in VL than in AL hiPSC-CMs, especially its inward component, which could explain the greater sensitivity of VL hiPSC-CM to I_f changes. By blocking I_f, the reduced

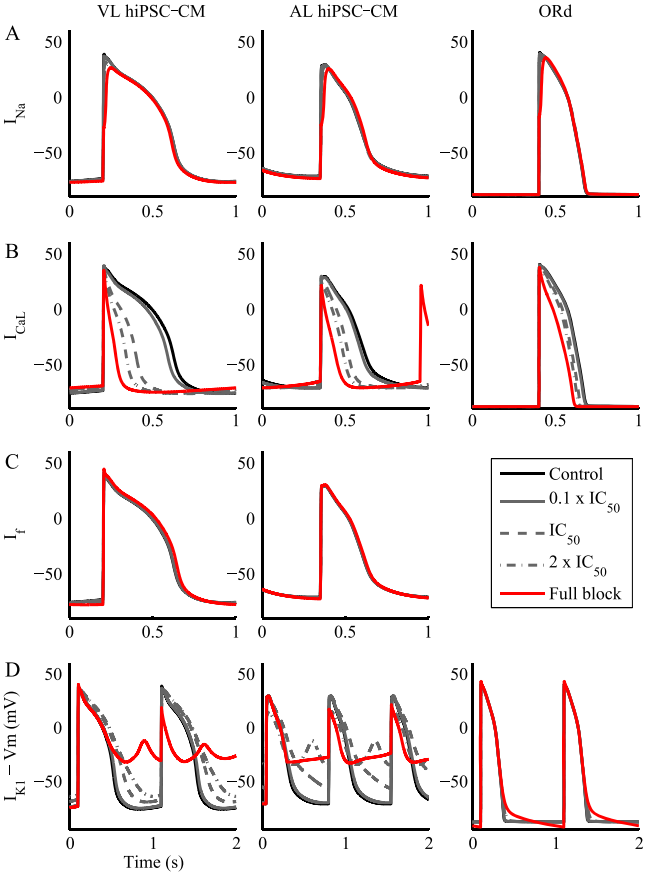

Figure 3

Comparison of the steady-state effects on the action potential of ionic current block in the VL (left) and AL (centre) hiPSC-CM and hAdultV-CM (right) models. The four blocker concentrations considered were as follows: 0.1 × IC_{50} = 9%, IC_{50} = 50%, 2 × IC_{50} = 67% and full block. I_f block was not simulated for hAdultV-CM model because it does not contain this current. VL and AL hiPSC-CM I_{K1} full block trace refers to the first APs after the block.

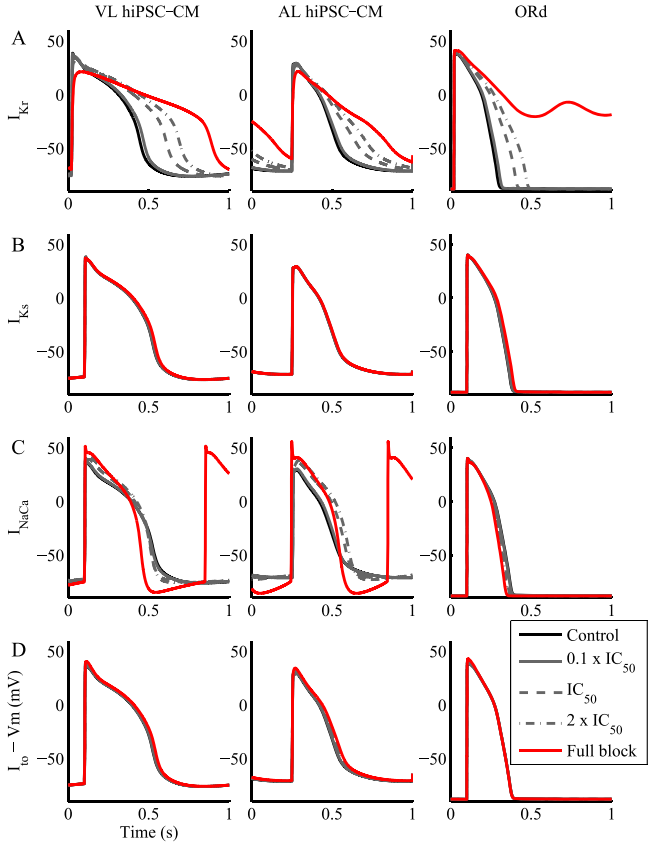

Figure 4

Comparison of the steady-state effects on the action potential of ionic current block in the VL (left) and AL (centre) hiPSC-CM and hAdultV-CM (right) models. The four blocker concentrations considered were as follows: 0.1 × IC_{50} = 9%, IC_{50} = 50%, 2 × IC_{50} = 67% and full. For all the models, I_{Kr} traces report AP after 7 s from block. I_{NaCa} full block traces refer to 10 beats after block.

inward component hyperpolarizes MDP up to 3%; especially for VL hiPSC-CM: this is reflected in an increased V_{Max} and peak voltage.

I_{NaCa} block. In Paci *et al.*, (2012), nickel was used to block the I_{NaCa}, but it also affected I_{Kr} and the T-type Ca^{2+} current. Recently, the effect of the more specific I_{NaCa} blocker ORM10103 was tested on canine ventricular cells, but its effects in human ventricular myocytes are still unknown (Kormos *et al.*, 2014; Nagy *et al.*, 2014). The most important effect caused by I_{NaCa} block (Figure 4C and Tables 2, S1, S2, S4 and S5) in *in silico* hiPSC-CMs and in hAdultV-CM, especially at full block, is the APD_{90} shortening, up to 20% in VL hiPSC-CM. In VL and AL hiPSC-CMs, we also observed a lot of additional effects. At full block, MDP was hyperpolarized because of the lack of the inward component of I_{NaCa}; this hyperpolarization induced a greater activation of I_{Na} and consequently a greater V_{Max}; moreover, as a consequence of the hyperpolarized MDP the I_{NaCa} block affected the whole AP morphology, with an increased peak voltage and the plateau phase moved towards more positive potentials and a slower repolarization, which made the APD_{30} and APD_{50} longer. Conversely, the phase 3 repolarization was faster and induced APD_{90} shortening. The phase 2 change was even more pronounced in AL hiPSC-CM, leading to a longer plateau duration, which almost compensated for the shortening obtained during the late repolarization. The full block traces shown in Figure 4C for both the hiPSC-CM models and the hAdultV-CM model are illustrative of the I_{NaCa} block occurring 10 beats after blocker administration: traces at the steady-state were not considered because of reduced intracellular ion concentrations. Finally, Figures S6 and S7 show the effect of I_{NaCa} block on the intracellular Na^+ and Ca^{2+} concentrations.

I_{to} block. Results using selective I_{to} blockers are scarce. In de Haan *et al.* (2006), AVE0118 was reported to be specific for I_{to} but it also affects the ultrarapid K^+ current. I_{to} block resulted in only minor effects in VL and AL hiPSC-CMs (Figure 4D and Tables 2, S1, S2, S4 and S5), specifically it increased the peak voltage and APD_{90}, especially for AL hiPSC-CM. Also for the hAdultV-CM (Table S3), I_{to} block mainly induced an

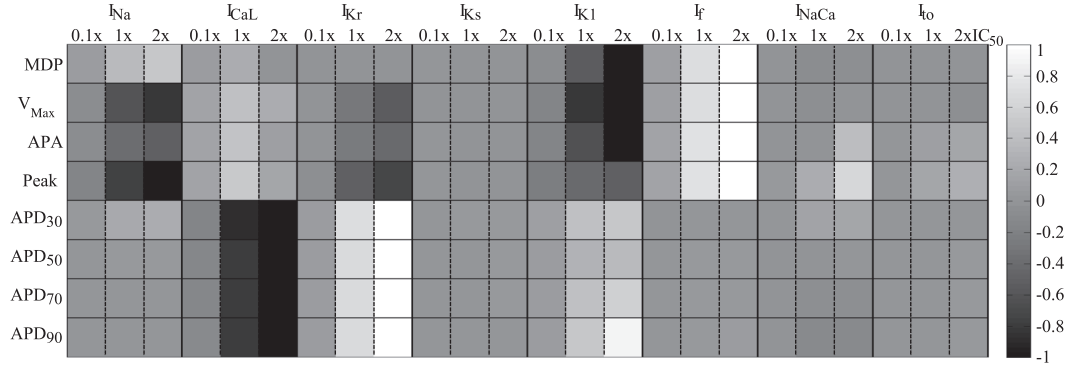

Figure 5

Global comparison of the effect of ionic current blocks on the morphological AP biomarkers simulated by the VL hiPSC-CM model. Stimulated APs were considered (pacing rate 60 beats min^{-1}). Grey levels represent the % variation of each biomarker (normalized in the interval [−1, 1], black: greatest reduction, white: greatest increment) for each block level. For I_{Kr}, biomarkers were computed 7 s after block, because for 2 × IC_{50} the AP was prolonged over the next stimulation pulse. APD_{xx}, action potential duration at XX% of repolarization.

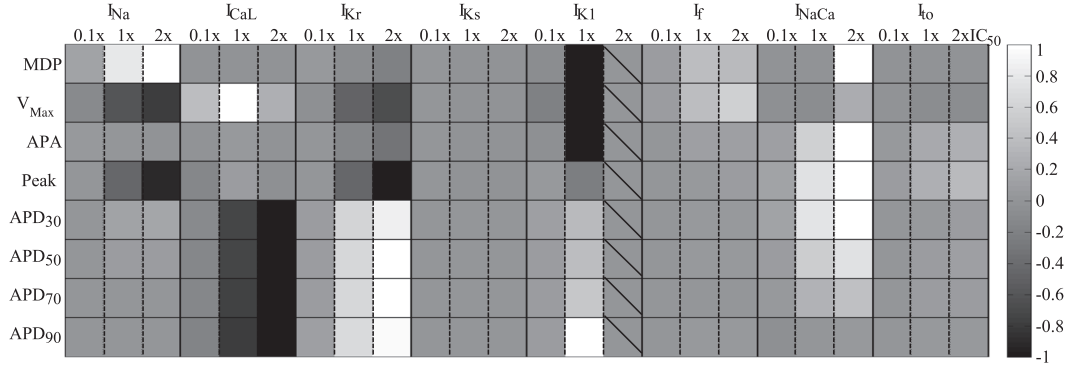

Figure 6

Global comparison of the effect of ionic current blocks on the morphological AP biomarkers simulated by the atrial-like hiPSC-CM model. Stimulated APs were considered (pacing rate 80 beats min^{-1}). Grey levels represent the % variation of each biomarker (normalized in the interval [−1, 1], black: greatest reduction, white: greatest increment) for each block level. 2 × IC_{50} was not considered for I_{K1} due to repolarization failure. For I_{Kr}, biomarkers were computed 7 s after block, because for 2 × IC_{50} the AP was prolonged over the next stimulation pulse. APD_{xx}, action potential duration at XX% of repolarization.

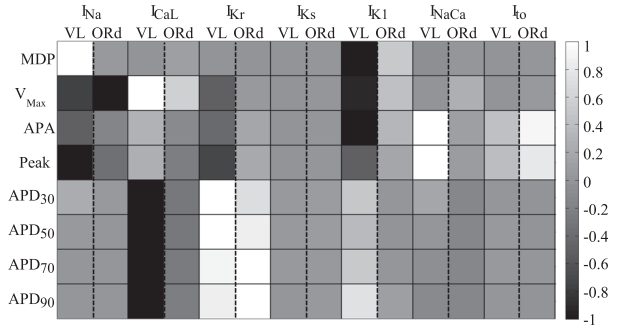

Figure 7

Comparison of the normalized % variation of the biomarkers induced by the blocker concentration 2 × IC_{50} in the VL hiPSC-CM and the hAdultV-CM (ORd) models. Biomarkers for I_{Kr} blocks were computed after 7 s from administration. APD_{xx}, action potential duration at XX% of repolarization.

increased peak voltage. I_{to} block would be expected to induce stronger effects in epicardial hAdultV-CM with a stronger I_{to} than the endocardial hAdultV-CM considered here.

Discussion

The present study provides a first systematic *in silico* evaluation of the effect of selective ionic current block on the AP shape of VL and AL hiPSC-CMs, and their comparison to hAdultV-CM. Quantitative results on AP biomarkers for the three cell types are obtained for four block levels of the eight most important transmembrane cardiac currents. Our main findings are as follows: (i) specific ionic current block induces similar qualitative changes in hiPSC-CMs and hAdultV-CM AP biomarkers for most ionic currents; (ii) given the importance of I_{Kr} block in preclinical drug evaluation, our results highlight that I_{Kr} block results in nearly

identical AP prolongation in VL hiPSC-CM and hAdultV-CM for 0.1 × IC_{50} and $IC_{50,}$ and consistent for 2 × IC_{50}; (iii) hiPSC-CMs were more sensitive to I_{CaL} and I_{K1} block, compared with hAdultV-CMs, for example, APD shortening/prolongation was up to more than four times larger after I_{CaL}/I_{K1} block; (iv) high levels of I_{K1} block induced repolarization failure in hiPSC-CMs, which was not observed in hAdult-CM (this increased sensitivity can be attributed to a reduced repolarization reserve of hiPSC-CMs); (v) our mechanistic study revealed the importance of differences in I_{NaCa}, I_{NaL} and I_{K1} between hAdult-CM and hiPSC-CMs in modulating their response to ionic current block. Although AL cells are present in *in vitro* preparations, they are a less common phenotype compared with the VL ones, and they are rarely used for drug tests. Therefore, greater attention was placed in this study on the VL hiPSC-CM model and its comparison to hAdultV-CM. However, we consider the presentation of the AL hiPSC-CM simulations useful, especially in the perspective of multicellular aggregates (e.g. multielectrode array and field potential).

By revealing differences and similarities in the sensitivity of hiPSC-CMs and hAdultV-CM to ionic current block, our analysis aims to help in the interpretation of further *in vitro* assays. We therefore expect the results of our investigations to support the currently developing synergy between *in vitro* and *in silico* approaches in the field of pharmacology and facilitate further development and use of hiPSC-CMs as a powerful *in vitro* technology for pharmacological applications in drug development and prescreening, which can be extended to take into consideration patient- and pathology-specificity.

hiPSC technology

Human-induced pluripotent stem cell-derived cardiomyocytes are likely to revolutionize drug testing as their production and use is more convenient and practical than harvesting human adult cells for *in vitro* studies, especially for non-diseased subjects. Further, they could contribute to the reduction, refinement and replacement of animal experimentation.

Human-induced pluripotent stem cell-derived cardiomyocytes have already proved their value as *in vitro* models for investigations into specific pathologies (Moretti *et al.*, 2010; Egashira *et al.*, 2012; Kujala *et al.*, 2012; Terrenoire *et al.*, 2013), and due to their patient-specificity, in identifying drugs for specific diseases (Itzhaki *et al.*, 2011, 2012; Matsa *et al.*, 2011; Yazawa *et al.*, 2011; Jung *et al.*, 2012), even though none of them has yet been administered to patients (Knollmann, 2013). Further advances in the development and application of the hiPSC technology for personalized therapies, however, require an in-depth and systematic evaluation of hiPSC-CMs and their maturity with a quantitative comparison with hAdultV-CM, which can be facilitated by *in silico* investigations such as the one presented in this study.

The majority of the most recently published datasets shows not only a high variability in the proposed APs (Table 3), but also immature phenotypes, for example, characterized by spontaneous APs and depolarized MDP. This leads to the still-open question "how similar are hiPSC-CMs to adult CMs?" and our study provides the first systematic study to aid in the characterization of similarities and differences.

Effect of ionic current block on hiPSC-CMs APs

Selective ionic current block was simulated by reducing the maximum conductance, using a simple pore block model. To investigate dose-dependency of the effects, four degrees of block were applied for each current. Previous studies (Romero *et al.*, 2009, 2011; Pueyo *et al.*, 2010; Christophe, 2013; Zemzemi *et al.*, 2013) have followed a similar approach to systematically investigate the sensitivity of AP biomarkers to specific ion channel changes. This approach was chosen because (i) selective blocks are important for cardiac drug discovery and (ii) it allows a controlled and systematic comparison between different cell types or models, which is a preliminary step before extending the analysis to more complex drug effects including multichannel actions.

In our study, VL hiPSC-CMs and hAdultV-CMs action potentials were simulated using the most comprehensive human models consistent with a large range of human data. Our new results showed a qualitatively similar response to current block between both cell types in several cases: (i) I_{Na} block induced a reduction of V_{Max}, peak voltage and AP amplitude; (ii) I_{CaL} block shortened the APD; (iii) I_{Kr} block prolonged the APD; (iv) I_{to} block increased the peak voltage; and (v) low sensitivity was found to I_{Ks} block. Nevertheless, quantitative differences were identified, such as (i) I_{CaL} block shortened APD more in hiPSC-CMs than in hAdultV-CM and (ii) I_{K1} block elevated MDP in hiPSC-CMs but not in

Table 3

Comparison between four datasets to show the variability inherent with VL hiPSC-CM measurements

	Ma2011	Moretti2010	Lahti2011	Ma2013
Rate (beats min^{-1})	35 ± 2	68 ± 3	72 ± 6	69 ± 11
MDP (mV)	−76 ± 1	−64 ± 2	−63 ± 1	−61 ± 1
APD_{90} (ms)	415 ± 22	381 ± 35	314 ± 18	434 ± 31

VL, ventricular-like; hiPSC-CM, human-induced pluripotent stem cell-derived cardiomyocyte; APD, action potential duration; MDP, maximum diastolic potential.

Ma2011 (Ma *et al.*, 2011) includes data from control hiPSC-CMs, used to record currents (I_{Na}, I_{CaL}, I_f, I_{to}, I_{Kr}, I_{Ks} and I_{K1}), spontaneous APs and response to selective blocks of I_{Na}, I_{CaL}, I_{Kr} and I_{Ks}. Moretti2010 (Moretti *et al.*, 2010) includes AP (spontaneous and stimulated) and current data (I_{Ks} and I_{Kr}) from control and patient cells to study the effects of LQT1. Lahti2011 (Lahti *et al.*, 2012) shows I_{Kr} and the spontaneous APs from control and patient hiPSC-CMs for LQT2 assessment. Ma2013 (Ma *et al.*, 2013) focuses on control and patient hiPSC-CMs to characterize the effects of LQT3, analysing APs and the fast and late I_{Na}.

hAdultV-CM. The mechanisms underlying such similarities and differences were investigated and discussed in the following by using the AP models for specifically designed simulations, which provide a powerful tool to unravel the underlying ionic mechanisms.

Ionic mechanisms underlying hiPSC-CM versus hAdultV-CM similarities and differences

The first main difference we observed between VL hiPSC-CM and hAdultV-CM is the stronger APD reduction, induced by I_{CaL} block, in the first model than in the second one. After testing many hypotheses, for example, the influence of the intracellular Na^+ and Ca^{2+} concentrations, and removing one by one the currents from the hAdultV-CM model to assess their contribution in case of I_{CaL} block, we found that the different extent of APD shortening is mainly due to the different I_{NaCa} formulations and to the presence in hAdultV-CM of I_{NaL}. Concerning I_{NaCa}, we performed the following *in silico* experiment: we transplanted the hiPSC-CM formulation of I_{NaCa} into the hAdultV-CM model, to evaluate its importance in the observed differences. Of note, this is one of the main advantages of *in silico* modelling, which allows in a relative short time to simulate phenomena and mechanisms too hard or time-consuming to test *in vitro*. In this sense, the computational analysis offers an interesting mechanistic insight into why the response of the hiPSC-CMs can be different from that of the adult cells: overexpression of I_{NaCa} can magnify the effects of I_{CaL} block. Actually, I_{NaCa} overexpression in incompletely mature CMs, and thus in hiPSC-CMs too, is still a matter of debate. Experiments in different animal models show the maximal I_{NaCa} density being reduced during maturation (Itoh *et al.*, 2007). The same trend is also maintained in human cells, where the expression of I_{NaCa} is higher at the mid-gestation than at the adult stage (Qu *et al.*, 2000). In cardiomyocytes derived from human pluripotent cells, in particular embryonic, it is reported how the I_{NaCa} expression is larger than in fetal and adult cells (Liu *et al.*, 2007; Li *et al.*, 2013) and it was confirmed by the current measurements reported in Paci *et al.* (2012), where I_{NaCa} is shown to be greater at the early developmental stage (15–40 days). However, in Fu *et al.* (2010), I_{NaCa} was reported to be greater at 90 days than at 40 days post-differentiation. Our simulation results point out the need for experimental data quantifying this aspect.

The second contribution to the preserved APD in hAdultV-CM after I_{CaL} block comes from I_{NaL}. Indeed, this current is included in the hAdultV-CM model, whereas it is not in the hiPSC-CM one, which is mainly based on the data of Ma *et al.* (2011), where no I_{NaL} was reported. The lack of this influx of positive charges delegates the support of the AP plateau phase to I_{CaL}, whose block has stronger effects in VL hiPSC-CM than in hAdultV-CM. Because I_{NaL} has been reported in hiPSC-CMs (Ma *et al.*, 2013), in this case, simulation results point out the need for the experimental characterization of this current and its inclusion in the hiPSC-CMs mathematical models.

The second main difference we observed between hiPSC-CM and hAdultV-CM is the extent of the effects of I_{K1} block, which confirms the critical role played by a non-completely mature I_{K1} in stem cells-derived CMs, in which instability of diastolic potential leads to spontaneous depolarization. Our results show that I_{K1} block results in significant effects on MDP and APD_{90} in VL hiPSC-CM, whereas in hAdultV-CM, MDP remains unaffected and APD_{90} prolongation is modest (<10%). We ascribe the greater sensitivity to I_{K1} blockade of VL hiPSC-CM to a reduced reserve of repolarization (Carmeliet, 2006): in hiPSC-CM, I_{Kr} is not able to carry out properly those compensatory mechanisms that in hAdultV-CM allow the reduction of the I_{K1} block effects.

For cardiotoxicity studies, the greater sensitivity of hiPSC-CM to drug blocks could be regarded as a useful feature providing clearly detectable indications about how a specific compound affects the cell electrophysiology. However, as shown by our study and *in vitro* experiments (Ma *et al.*, 2011; Knollmann, 2013), it is also an important indicator of the fact that the cells the Paci2013 model is based on, and more in general hiPSC-CMs, were not behaving exactly like adult cells, thus particular care should be used when considering them as fully representative models of adult cells. This oversensitivity is something to be aware of, but not enough to dismiss hiPSC-CMs as an inadequate model. We know indeed that every *in vivo*, *in vitro* or *in silico* model has advantages and disadvantages in the translation of its results to humans. If anything, this highlights the importance of further studies to achieve better and more effective maturation, characterization and possibly improve (e.g. I_{K1} overexpression) hiPSC-CMs. The final goal is an integrated approach, in which compounds are tested in real hiPSC-CMs, whereas *in silico* simulations with both hiPSC-CM and hAdultV-CM will help in interpreting and translating the results to real adult cells *in vivo*. Thus, decisions should be taken from data obtained by running in parallel *in silico* and *in vitro* experiments on hiPSC-CMs and taking into account both sets of result. It will improve the degree of awareness of hiPSC-CM descriptive power: if results are consistent, the confidence in them will be higher, otherwise the interpretation of the results should be treated with caution. This scenario also represents a typical field for the application of the new concept of model-simulation-experiment (MSE) system (Carusi *et al.*, 2012). In this regard models, simulations and experiments are interlaced in a synergic assemblage, whose expressive power for the representation of biological mechanisms progressively grows, as the MSE system itself is constructed.

A further step for cardiotoxicity studies consists in analysing and integrating different levels of details into a multiscale approach. In fact, in order to get an overall understanding of arrhythmogenic mechanisms and how new compounds could affect them, the integration of measurements and simulations at the cellular, tissue, organ and even *in vivo* levels is essential.

Potential applications of our methodology are as follows: (i) *in silico* experiments aimed at evaluating stem cell-derived CM maturity, for example, by replacing single or multiple ionic currents with their adult versions, in order to compare hiPSC-CM models with hybrid or partially adult models; (ii) the investigation of the observed high *in vitro* variability by means of *in silico* models derived from patient-specific and disease-specific hiPSC-CMs, for example exploiting specific

populations of models (Britton *et al.*, 2013; Gemmell *et al.*, 2014); and (iii) the analysis of the already known differences between hiPSC-CMs and hAdultV-CMs, for example, assessing the impact of a reduced repolarization reserve on *in vitro* models of arrhythmogenic pathologies.

Future work and limitations

A comparison of published datasets highlights the surprisingly high variability in the APs measured during experiments in hiPSC-CMs. In the light of such large variations in measurements and cell lines, the construction of *in-silico* models requires an informed choice on the experimental data to be considered and integrated. In Paci *et al.* (2013a), the hiPSC-CM models were based on the comprehensive dataset reported in Ma *et al.* (2011), giving only secondary consideration to additional datasets. Of note, this dataset is based on measurements from isolated iCell hiPSC-CMs by Cellular Dynamics International; therefore, the Paci2013 model reproduces the electrophysiological behaviour of isolated hiPSC-CMs from this specific commercial line. Other commercial hiPSC-CMs lines are available (e.g. Cor.4U by Axiogenesis) and many more are produced in single laboratories, thus line-to-line variability is an issue. Moreover, hiPSC-CM biomarkers are dependent on the measurement conditions, for example, isolated cell patch-clamp versus microelectrode arrays on monolayers. Consequently, a possible limitation of the present study is the general applicability of our results to hiPSC-CMs obtained in different laboratories and/or from different cell lines, suggesting that specific *in silico* models should be tailored for different hiPSC-CM lines. However, it is worth noting that the Paci2013 hiPSC-CM model already comprises the flexibility to reproduce datasets from cell lines different from the one used to develop the model. In Paci *et al.* (2013b, 2014), we showed how, with few changes in the maximal conductances of the ion currents, we reproduced different control APs. Moreover, integrating mutation-specific data, mutant LQT1 and LQT3 APs were also properly reproduced. These results suggest that the intrinsic behaviour of the cells, and eventually their response to current blockers, could be more conserved than the more commonly measured AP features. Nevertheless, as reported earlier, this aspect needs to be investigated in more depth, for example, by exploiting the populations of models approach.

In this study, we have considered single pore block models, and this approach has proved useful in previous studies (Brennan *et al.*, 2009; Zemzemi *et al.*, 2013). It includes important information on cardiac sensitivity to drug effects and can be extended to drugs with multichannel actions. In the case of hiPSC-CMs, however, the situation is even more complex: indeed, for adult cells, studies have published IC_{50} for different drugs, and also for multiple channels (Mirams *et al.*, 2011; Davies *et al.*, 2012). At present, the same kind of information is not available for hiPSC-CMs but our studies could be extended once comparable *in vitro* data become available for hiPSC-CMs. Furthermore, our work focuses on the effect of ionic current block on AP biomarkers rather than EADs and those were observed only for very high degrees of I_{Kr} block in hAdultV-CM. In the case of hiPSC-CMs, the observed high variability reported in the literature also affects the presence of EADs. In particular, in the literature, the occurrence of EADs is reported to be variable (Hoekstra *et al.*, 2012) and generally in specific stimulation conditions (e.g. very slow pacing rate such as 30 beats min^{-1}). Moreover, generally not all the cells tested showed the occurrence of EADs, but only a subset of them showed repolarization anomalies (Ma *et al.*, 2011). Variations in the occurrence of EADs were observed not only in control cells but also in mutant hiPSC-CMs derived from patients, for example, in conditions of impaired I_{Kr} by LQT2 syndrome: in Lahti *et al.* (2012), EADs were observed, but not by Bellin *et al.* (2013). It seems, therefore, that in order to reliably assess the occurrence of this kind of pro-arrhythmia marker, the intercellular variability should also be taken into account in the computational models. Further studies can extend our hiPSC-CMs models to investigate mechanisms of EADs generation. Finally, our modelling approach could also be extended to include more complex models of drug/ion channel interactions, specifically when drug-induced effects on current kinetics need to be evaluated (Di Veroli *et al.*, 2013; Romero *et al.*, 2014).

Conclusions

This study presents the first application of hiPSC-CM *in silico* models for the assessment and comparison of the effects of specific current block on hiPSC-CM and hAdultV-CM APs. Qualitatively, the response of all cell types was overall similar but an increased sensitivity was observed with the hiPSC-CMs, specifically to I_{CaL} and I_{K1} block. Quantitatively, we showed how the increased sensitivity of the hiPSC-CMs was mainly due to the overexpression of I_{NaCa} in the case of I_{CaL} block, whereas it was due to the reduced repolarization reserve in the case of I_{K1} block. Our results are potentially useful for developing synergistic approaches for pharmacological investigations, using combined *in silico* and *in vitro* hiPSC-CM technologies for safety assessments and target identification during drug development.

Acknowledgements

M. P. was financially supported by Tekes, Finland (decision: 40346/11) and by the Finnish Cultural Foundation, Central Fund, Finland. B. R. holds a Wellcome Trust Senior Research Fellowship in Basic Biomedical Science.

Author contributions

M. P. conducted the experiments, analysed/interpreted data and wrote the article. J. H. designed the experiments, analysed/interpreted data and proofed/revised the article. B. R. designed the experiments, analysed/interpreted data, wrote the article and proofed/revised the article. S. S. designed the experiment, analysed/interpreted data and proofed/revised the article.

Conflict of interest

None.

References

Alexander SPH, Benson HE, Faccenda E, Pawson AJ, Sharman JL, Spedding M *et al.* (2013a). The Concise Guide to PHARMACOLOGY 2013/14: G protein-coupled receptors. Br J Pharmacol 170: 1459–1581.

Alexander SPH, Benson HE, Faccenda E, Pawson AJ, Sharman JL, Spedding M *et al.* (2013b). The Concise Guide to PHARMACOLOGY 2013/14: transporters. Br J Pharmacol 170: 1706–1796.

Bellin M, Casini S, Davis RP, D'Aniello C, Haas J, Ward-van Oostwaard D *et al.* (2013). Isogenic human pluripotent stem cell pairs reveal the role of a KCNH2 mutation in long-QT syndrome. EMBO J 32: 3161–3175.

Brennan T, Fink M, Rodriguez B (2009). Multiscale modelling of drug-induced effects on cardiac electrophysiological activity. Eur J Pharm Sci 36: 62–77.

Britton OJ, Bueno-Orovio A, Van Ammel K, Lu HR, Towart R, Gallacher DJ *et al.* (2013). Experimentally calibrated population of models predicts and explains intersubject variability in cardiac cellular electrophysiology. Proc Natl Acad Sci U S A 110: E2098–E2105.

Carmeliet E (2006). Repolarization reserve in cardiac cells. J Med Biol Eng 26: 97–105.

Carusi A, Burrage K, Rodríguez B (2012). Bridging experiments, models and simulations: an integrative approach to validation in computational cardiac electrophysiology. Am J Physiol Heart Circ Physiol 303: H144–H155.

Christophe B (2013). Simulation of early after-depolarisation in non-failing human ventricular myocytes: can this help cardiac safety pharmacology? Pharmacol Rep 65: 1281–1293.

Davies MR, Mistry HB, Hussein L, Pollard CE, Valentin J-P, Swinton J *et al.* (2012). An *in silico* canine cardiac midmyocardial action potential duration model as a tool for early drug safety assessment. AJP - Heart Circ Physiol 302: H1466–H1480.

Egashira T, Yuasa S, Suzuki T, Aizawa Y, Yamakawa H, Matsuhashi T *et al.* (2012). Disease characterization using LQTS-specific induced pluripotent stem cells. Cardiovasc Res 95: 419–429.

Fu J-D, Jiang P, Rushing S, Liu J, Chiamvimonvat N, Li RA (2010). Na+/Ca2+ exchanger is a determinant of excitation-contraction coupling in human embryonic stem cell-derived ventricular cardiomyocytes. Stem Cells Dev 19: 773–782.

Gemmell P, Burrage K, Rodriguez B, Quinn TA (2014). Population of computational rabbit-specific ventricular action potential models for investigating sources of variability in cellular repolarisation. PLoS One 9: e90112.

de Haan S, Greiser M, Harks E, Blaauw Y, van Hunnik A, Verheule S *et al.* (2006). AVE0118, blocker of the transient outward current (I(to)) and ultrarapid delayed rectifier current (I(Kur)), fully restores atrial contractility after cardioversion of atrial fibrillation in the goat. Circulation 114: 1234–1242.

Hamdam J, Sethu S, Smith T, Alfirevic A, Alhaidari M, Atkinson J *et al.* (2013). Safety pharmacology–current and emerging concepts. Toxicol Appl Pharmacol 273: 229–241.

Heist EK, Ruskin JN (2010). Drug-induced arrhythmia. Circulation 122: 1426–1435.

Hoekstra M, Mummery CL, Wilde A a M, Bezzina CR, Verkerk AO (2012). Induced pluripotent stem cell derived cardiomyocytes as models for cardiac arrhythmias. Front Physiol 3: 346.

Itoh H, Naito Y, Tomita M (2007). Simulation of developmental changes in action potentials with ventricular cell models. Syst Synth Biol 1: 11–23.

Itzhaki I, Maizels L, Huber I, Gepstein A, Arbel G, Caspi O *et al.* (2012). Modeling of catecholaminergic polymorphic ventricular tachycardia with patient-specific human-induced pluripotent stem cells. J Am Coll Cardiol 60: 990–1000.

Itzhaki I, Maizels L, Huber I, Zwi-Dantsis L, Caspi O, Winterstern A *et al.* (2011). Modelling the long QT syndrome with induced pluripotent stem cells. Nature 471: 225–229.

Jung CB, Moretti A, Mederos y Schnitzler M, Iop L, Storch U, Bellin M *et al.* (2012). Dantrolene rescues arrhythmogenic RYR2 defect in a patient-specific stem cell model of catecholaminergic polymorphic ventricular tachycardia. EMBO Mol Med 4: 180–191.

Kannankeril P (2010). Drug-induced long QT syndrome. Pharmacol Rev 62: 760–781.

Knollmann BC (2013). Induced pluripotent stem cell-derived cardiomyocytes: boutique science or valuable arrhythmia model? Circ Res 112: 969–976.

Kormos A, Nagy N, Acsai K, Váczi K, Ágoston S, Pollesello P *et al.* (2014). Efficacy of selective NCX inhibition by ORM-10103 during simulated ischemia/reperfusion. Eur J Pharmacol 740: 539–551.

Kujala K, Paavola J, Lahti A, Larsson K, Pekkanen-Mattila M, Viitasalo M *et al.* (2012). Cell model of catecholaminergic polymorphic ventricular tachycardia reveals early and delayed afterdepolarizations. PLoS One 7: e44660.

Lahti AL, Kujala VJ, Chapman H, Koivisto A-P, Pekkanen-Mattila M, Kerkela E *et al.* (2012). Model for long QT syndrome type 2 using human iPS cells demonstrates arrhythmogenic characteristics in cell culture. Dis Model Mech 5: 220–230.

Leishman DJ, Beck TW, Dybdal N, Gallacher DJ, Guth BD, Holbrook M *et al.* (2012). Best practice in the conduct of key nonclinical cardiovascular assessments in drug development: current recommendations from the Safety Pharmacology Society. J Pharmacol Toxicol Methods 65: 93–101.

Li G, Feng J, Yue L, Carrier M (1998). Transmural heterogeneity of action potentials and Ito1 in myocytes isolated from the human right ventricle. Am J Physiol 275: H369–H377.

Li S, Chen G, Li RA (2013). Calcium signaling of human pluripotent stem cell-derived cardiomyocytes. J Physiol 591: 5279–5290.

Liu J, Fu JD, Siu CW, Li RA (2007). Functional sarcoplasmic reticulum for calcium handling of human embryonic stem cell-derived cardiomyocytes: insights for driven maturation. Stem Cells 25: 3038–3044.

Ma D, Wei H, Zhao Y, Lu J, Li G, Binte N *et al.* (2013). Modeling type 3 long QT syndrome with cardiomyocytes derived from patient-specific induced pluripotent stem cells. Int J Cardiol 168: 5277–5286.

Ma J, Guo L, Fiene SJ, Anson BD, Thomson JA, Kamp TJ *et al.* (2011). High purity human-induced pluripotent stem cell-derived cardiomyocytes: electrophysiological properties of action potentials and ionic currents. AJP - Heart Circ Physiol 301: H2006–H2017.

Matsa E, Rajamohan D, Dick E, Young L, Mellor I, Staniforth A *et al.* (2011). Drug evaluation in cardiomyocytes derived from human induced pluripotent stem cells carrying a long QT syndrome type 2 mutation. Eur Heart J 32: 952–962.

Mirams GR, Cui Y, Sher A, Fink M, Cooper J, Heath BM *et al.* (2011). Simulation of multiple ion channel block provides improved early prediction of compounds' clinical torsadogenic risk. Cardiovasc Res 91: 53–61.

Moretti A, Bellin M, Welling A, Jung CB, Lam JT, Bott-Flügel L *et al.* (2010). Patient-specific induced pluripotent stem-cell models for long-QT syndrome. N Engl J Med 363: 1397–1409.

Nagy N, Kormos A, Kohajda Z, Szebeni Á, Szepesi J, Pollesello P *et al.* (2014). Selective Na(+) /Ca(2+) exchanger inhibition prevents Ca(2+) overload-induced triggered arrhythmias. Br J Pharmacol 171: 5665–5681.

O'Hara T, Virág L, Varró A, Rudy Y (2011). Simulation of the undiseased human cardiac ventricular action potential: model formulation and experimental validation. PLoS Comput Biol 7: e1002061.

Paci M, Hyttinen J, Aalto-Setälä K, Severi S (2013a). Computational models of ventricular- and atrial-like human induced pluripotent stem cell derived cardiomyocytes. Ann Biomed Eng 41: 2334–2348.

Paci M, Hyttinen J, Severi S (2013b). Computational modelling of LQT1 in human induced pluripotent stem cell derived cardiomyocytes. Comput Cardiol 40: 1239–1242.

Paci M, Sartiani L, Lungo M, Jaconi M, Mugelli A, Cerbai E *et al.* (2012). Mathematical modelling of the action potential of human embryonic stem cell derived cardiomyocytes. Biomed Eng Online 11: 61.

Paci M, Severi S, Hyttinen J (2014). Computational modeling supports induced pluripotent stem cell-derived cardiomyocytes reliability as a model for human LQT3. Comput Cardiol 41: 69–72.

Pawson AJ, Sharman JL, Benson HE, Faccenda E, Alexander SP, Buneman OP *et al.* (2014). The IUPHAR/BPS Guide to PHARMACOLOGY: an expert-driven knowledgebase of drug targets and their ligands. Nucl. Acids Res. 42 (Database Issue): D1098–106.

Pueyo E, Husti Z, Hornyik T (2010). Mechanisms of ventricular rate adaptation as a predictor of arrhythmic risk. AJP - Heart Circ Physiol 298: H1577–H1587.

Qu Y, Ghatpande A, El-Sherif N, Boutjdir M (2000). Gene expression of Na+/Ca2+ exchanger during development in human heart. Cardiovasc Res 45: 866–873.

Rodriguez B, Burrage K, Gavaghan D, Grau V, Kohl P, Noble D (2010). The systems biology approach to drug development: application to toxicity assessment of cardiac drugs. Clin Pharmacol Ther 88: 130–134.

Romero L, Carbonell B, Trenor B, Rodríguez B, Saiz J, Ferrero JM (2011). Systematic characterization of the ionic basis of rabbit cellular electrophysiology using two ventricular models. Prog Biophys Mol Biol 107: 60–73.

Romero L, Pueyo E, Fink M, Rodriguez B (2009). Impact of ionic current variability on human ventricular cellular electrophysiology. AJP Heart Circ Physiol 297: H1436–H1445.

Romero L, Trenor B, Yang P-C, Saiz J, Clancy CE (2014). *In silico* screening of the impact of hERG channel kinetic abnormalities on channel block and susceptibility to acquired long QT syndrome. J Mol Cell Cardiol 72: 126–137.

Sager PT, Gintant G, Turner JR, Pettit S, Stockbridge N (2014). Rechanneling the cardiac proarrhythmia safety paradigm: a meeting report from the Cardiac Safety Research Consortium. Am Heart J 167: 292–300.

Sartiani L, Bettiol E, Stillitano F, Mugelli A, Cerbai E, Jaconi ME (2007). Developmental changes in cardiomyocytes differentiated from human embryonic stem cells: a molecular and electrophysiological approach. Stem Cells 25: 1136–1144.

Sauer AJ, Newton-Cheh C (2012). Clinical and genetic determinants of torsade de pointes risk. Circulation 125: 1684–1694.

Shah RR (2013). Drug-induced QT interval prolongation: does ethnicity of the thorough QT study population matter? Br J Clin Pharmacol 75: 347–358.

So PP-S, Backx PH, Dorian P (2008). Slow delayed rectifier K+ current block by HMR 1556 increases dispersion of repolarization and promotes Torsades de Pointes in rabbit ventricles. Br J Pharmacol 155: 1185–1194.

Terrenoire C, Wang K, Tung KWC, Chung WK, Pass RH, Lu JT *et al.* (2013). Induced pluripotent stem cells used to reveal drug actions in a long QT syndrome family with complex genetics. J Gen Physiol 141: 61–72.

Thomas G, Gerlach U, Antzelevitch C (2003). HMR 1556, a potent and selective blocker of slowly activating delayed rectifier potassium current. J Cardiovasc Pharmacol 41: 140–147.

Di Veroli GY, Davies MR, Zhang H, Abi-Gerges N, Boyett MR (2013). High-throughput screening of drug-binding dynamics to HERG improves early drug safety assessment. Am J Physiol Heart Circ Physiol 304: H104–H117.

Yazawa M, Hsueh B, Jia X, Pasca AM, Bernstein JA, Hallmayer J *et al.* (2011). Using induced pluripotent stem cells to investigate cardiac phenotypes in Timothy syndrome. Nature 471: 230–234.

Zemzemi N, Bernabeu MO, Saiz J, Cooper J, Pathmanathan P, Mirams GR *et al.* (2013). Computational assessment of drug-induced effects on the electrocardiogram: from ion channel to body surface potentials. Br J Pharmacol 168: 718–733.

Supporting Information

Additional Supporting Information may be found in the online version of this article at the publisher's web-site:

http://dx.doi.org/10.1111/bph.13282

Table S1a AP biomarkers changes induced by the different blockade levels in the stimulated ventricular-like model.
Table S1b AP biomarkers percent variations with respect to the control AP induced by the different blockade levels in the stimulated ventricular-like model.
Table S2a AP biomarkers changes induced by the different blockade levels in the stimulated atrial-like model.
Table S2b AP biomarkers percent variations with respect to the control AP induced by the different blockade levels in the stimulated atrial-like model.
Table S3a AP biomarkers changes induced by the different blockade levels in the adult ORd model (I_f not present in the ORd model).
Table S3b AP biomarkers percent variations with respect to the control AP induced by the different blockade levels in the adult ORd model.
Table S4 Comparison between spontaneous (gray) and stimulated (white) ventricular-like hiPSC-CM APs. Biomarkers are presented as percent variations with respect to the control AP induced by the different blockade levels in the stimulated ventricular-like model.
Table S5 Comparison between spontaneous (gray) and stimulated (white) atrial-like hiPSC-CM APs. Biomarkers are

presented as percent variations with respect to the control AP induced by the different blockade levels in the stimulated atrial-like model.

Figure S1 Details of the effect of I_{Na} block on the AP upstroke.

Figure S2 Global comparison of the effect of ionic current blocks on the morphological action potential (AP) biomarkers simulated by the hAdultV-CM model. The pacing rate is 60 bpm. Grey levels represent the percent variation of each biomarker (normalized in the interval [−1, 1]) for each block level. MDP: maximum diastolic potential, V_{Max}: maximum upstroke velocity, APA: action potential amplitude, Peak: peak voltage, APD_{xx}: action potential duration at XX% of repolarization.

Figure S3 I_f block effects on VL hiPSC-CM and hAL hiPSC-CM. In panels B and C the effects on MDP and Peak have been detailed, respectively.

Figure S4 Assessment of the different contributions that sustain the AP in the hAdultV-CM (ORd) model and comparison with full I_{CaL} block in VL hiMPSC-CM. Black, green and magenta traces refer to hAdultV-CM hybridized with the VL hiPSC-CM I_{NaCa}. The red trace refers to the hAdultV-CM model with its original I_{NaCa} formulation and a 3.2-fold increase in the maximal current.

Figure S5 Assessment of the repolarization reserve in VL hiPSC-CM and hAdultV-CM. A and B: comparison of different I_{K1} blocks on the APs and the underlying I_{Kr}. C: compensation of the I_{K1} block by doubling I_{Kr} (increment to 80 bpm of the pacing rate is needed to avoid spontaneous APs). D: the halved IKr and the consequent slower repolarization show how I_{Kr} compensates the absence of I_{K1} in adult cells.

Figure S6 Na^+ concentration in conditions of I_{NaCa} block.

Figure S7 Ca^{2+} concentration in conditions of I_{NaCa} block. Peak of hAdultV-CM Ca^{2+} transient equals to 0.022 mM.